Lagrangian Velocity Spectra at 700 m in the Western North Atlantic

VOLFANGO RUPOLO,* BACH LIEN HUA,+ ANTONELLO PROVENZALE,@ AND VINCENZO ARTALE*

*ENEA, CRE Casaccia, Rome, Italy
+Laboratoire de Physique des Oceans, UMR/CNRS, IFREMER, Plouzane, France
@Istituto di Cosmogeofisica, CNR Corso Fiume, Turin, Italy

(Manuscript received 22 May 1995, in final form 12 February 1996)

ABSTRACT

Pending an appropriate scaling of each trajectory by its Lagrangian integral timescale T_L, there exists a generic shape of the Lagrangian frequency spectrum for the trajectories of the 700-m dataset in western North Atlantic, which are stationary on the timescale of 200 days. The generic spectral shape contains a plateau at the lowest frequencies extending up to $\nu_0 \sim (30T_L)^{-1}$, a power-law behavior with an intermediate spectral slope $\alpha = 0.25$ between ν_0 and $\nu_1 \sim (3 \sim 4T_L)^{-1}$, and a steeper slope $n \geq 3$ at larger frequencies. Such a steep slope at large frequencies implies that most of Lagrangian dispersion can be ascribed to low and intermediate frequency motions. The variance of the Lagrangian acceleration computed from such a spectrum is finite, indicating continuous particle accelerations and supporting a truly Lagrangian behavior of the 700-m floats. The existence of an intermediate power-law behavior in the spectrum can be linked with the trapping of some trajectories by persistent energetic structures and is associated with a tendency for anomalous diffusion lasting up to $10T_L$. The authors also introduce an alternative method for computing T_L from a yardstick measure of Lagrangian decorrelation length from each individual trajectory.

1. Introduction

The purpose of this work is to revisit the 700-m historical Lagrangian dataset of the western North Atlantic (Richardson et al. 1981; Owens 1991) in order to look for generic properties of Lagrangian dispersion induced by the strong mesoscale turbulence ubiquitous at that depth (Price et al. 1987). We specifically examine the Lagrangian position structure function and we study how its behavior at both small and large time lags is determined by the various frequency bands in the Lagrangian kinetic energy spectrum.

The study of dispersion in mesoscale turbulence in the northwestern Atlantic is inherently arduous because of two main sources of difficulties: (i) the existence of inhomogeneities of the flow at the largest spatial scales and (ii) the diversity of regimes encompassed by the dataset.

In order to have sufficiently long time series, we discard the trajectories shorter than 200 days. Following this criterion, a total of 74 trajectories at 700 m have been retained. Since here we opt not to address dynamical issues linked with the large-scale spatial inhomogeneities of the flow, we then screen the 74 trajectories in order to retain only trajectories with stationary velocity fluctuations (section 2). To this end, we require the Lagrangian velocity spectrum to be equal to the position fluctuation spectrum multiplied by ν^2, where ν is the frequency (see discussion in appendix A). By this kinematic criterion, 56 trajectories at 700 m are retained. The excluded trajectories correspond to the 24% of the number of trajectories longer than 200 days and their behavior is presumably due to the inhomogeneities of the flow at the largest spatial scales. Here the focus is on mesoscale turbulence, thus we do not address the issue of large-scale spatial inhomogeneities.

The second source of difficulties is the great diversity of dynamical regimes of the stationary trajectories, with extreme behaviors corresponding respectively to energetic persistent structures (such as jets or vortices) and quiescent midocean conditions (section 2).

The existence of common spectral features between trajectories typical of the two extremes motivates the search of a characteristic spectrum representative of all of the stationary dataset. A key point of our approach is to perform an appropriate rescaling of both ordinate and abscissa of the Lagrangian kinetic energy spectrum for each trajectory. For that purpose we introduce an alternative method for evaluating the Lagrangian integral timescale T_L. This is based on first computing a correlation length through a yardstick measure of the length of the trajectory and then supplementing the approach with dimensional considerations (section 3). The motivation is that the usual spectral evaluation of T_L, based on the behavior of individual trajectories at the smallest frequencies (e.g., see Davis 1991), is not always well defined despite that individual trajectories

Corresponding author address: Dr. Bach Lien Hua, Laboratoire de Physique des Océans, IFREMER/Centre de Brest, B. P. 70, Plouzané 29280, France.

may pass the test of kinematic stationarity defined above.

The main result of this work is the obtention of a generic shape of the Lagrangian kinetic energy spectrum that is representative of those trajectories stationary on the timescale of 200 days (section 4). This spectral shape is characterized by a plateau at very small frequencies $\nu \leq \nu_0$ and a steep slope for $\nu > \nu_1$, where ν_0 and ν_1 are found to be respectively $\sim(30T_L)^{-1}$ and $(3 \sim 4\ T_L)^{-1}$.

The slope n appears to be steeper than 3. At intermediate frequencies, a distinct regime is observed that is characterized by a spectral slope $\alpha = 0.25$. The plateau at the smallest frequencies corresponds to the classical Brownian–Taylor dispersion (Taylor 1921), while the intermediate regime is associated with anomalous dispersion on these timescales. The large spectral slope at $\nu > \nu_1$ is associated with ballistic dispersion on times smaller than $1/\nu_1$.

This characteristic shape of the spectrum is in agreement with the results of direct numerical simulations of Lagrangian trajectories in geostrophic turbulence (Hua and McWilliams 1996, manuscript submitted to *J. Fluid Mech.*).

By using simple analytical fits to the generic Lagrangian velocity spectrum, we then search for its implications on the structure function of Lagrangian position, which is the usual estimator for characterizing dispersion (section 5). An important result is that the smallest and intermediate frequencies of Lagrangian kinetic energy have a predominant influence on the position structure function for the whole range of time lags whenever the velocity spectrum is steep enough.

A side issue of this work concerns the contrast between the Lagrangian velocity spectra and the Eulerian ones (e.g., see Davis 1983; Babiano et al. 1985, 1987) with a generally steeper slope for the Lagrangian spectra at high frequencies with respect to the observed Eulerian ones (Wunsch 1982). This result is dynamically compatible with the common observation that the Lagrangian integral timescale is shorter than its Eulerian counterpart (Middleton 1985).

Section 3, which gives the technical details for determining T_L, may be skipped by the reader who is more interested in the results of the spectral analysis and dispersion given in sections 4 and 5.

2. Stationary trajectories and their variability

The power spectrum of the (vector) velocity time series $\mathbf{u}(t)$ is defined as

$$P(\nu) = C[\mathbf{A}(\nu)\cdot\mathbf{A}^*(\nu)],$$

where ν is the frequency in *cpd*; the asterisk indicates complex conjugation, and

$$\mathbf{A}(\nu) = \int_{-\infty}^{+\infty} \mathbf{u}(t)e^{-i2\pi\nu t}dt.$$

The normalization constant C is defined by

$$\int_{-\infty}^{+\infty} P(\nu)d\nu = 1. \tag{1}$$

We have

$$P(\nu) = 2\int_0^{+\infty} R(t)\cos(2\pi\nu t)dt \tag{2}$$

and

$$R(\tau) = \lim_{T\to\infty}\frac{1}{T\sigma_u^2}\int_0^T \mathbf{u}'(t+\tau)\cdot\mathbf{u}'(t)dt,$$

where $R(\tau)$ is the autocorrelation function, $\mathbf{u}'(t)$ and σ_u^2 are respectively the velocity fluctuation and its variance. From (2) we obtain the Lagrangian integral time T_L

$$T_L = \int_0^{\infty} R(\tau)d\tau = \frac{1}{2}P(0). \tag{3}$$

If the velocity power spectrum $P(\nu)$ saturates at small frequencies, relation (3) can be used to estimate T_L.

In order to adequately resolve mesoscale dynamics (a typical order of magnitude of T_L being about 10 days; Owens 1991), we analyze trajectories that are longer than 200 days. Since the dynamical focus is on mesoscale turbulence, and in order to avoid difficulties inherently linked with large-scale spatial inhomogeneity, we seek to work with stationary velocity time series. The aim is to eliminate the trajectories that visit both high and low energy regions and to preserve only trajectories that do not display a mean trend in velocity over the timescale of 200 days, the trend being associated with the presence of a net mean acceleration induced by the inhomogeneity of the flow on spatial scales larger than those resolved by the data. The subsequent analysis is thus performed only on those individual trajectories that satisfy

$$P(\nu) = \nu^2 Q(\nu), \tag{4}$$

where $Q(\nu)$ is the power spectrum of $\mathbf{x}'(t) = \mathbf{x}(t) - \bar{\mathbf{u}}t$ and $\bar{\mathbf{u}}$ is the mean velocity of the float (given, e.g., by the slope of a linear least-square fit to the float position versus time). Relation (4) is a necessary condition for the stationarity of the velocity time series or, equivalently, for the stationarity of the increments of the position with time (Panchev 1971). We show in appendix A that (4) coincides with the requirement of no mean Lagrangian acceleration of the float trajectory. By the stationarity criterion, we retain 56 of the 74 trajectories that are longer than 200 days (Fig. 1). Note that the stationary data comes from only 41 distinct floats since we have cut some of the very long trajectories into pieces of 256 days. Note also that the definition of stationarity employed here does not necessarily imply the convergence of the individual kinetic energy spectra at low frequencies; as a matter of fact,

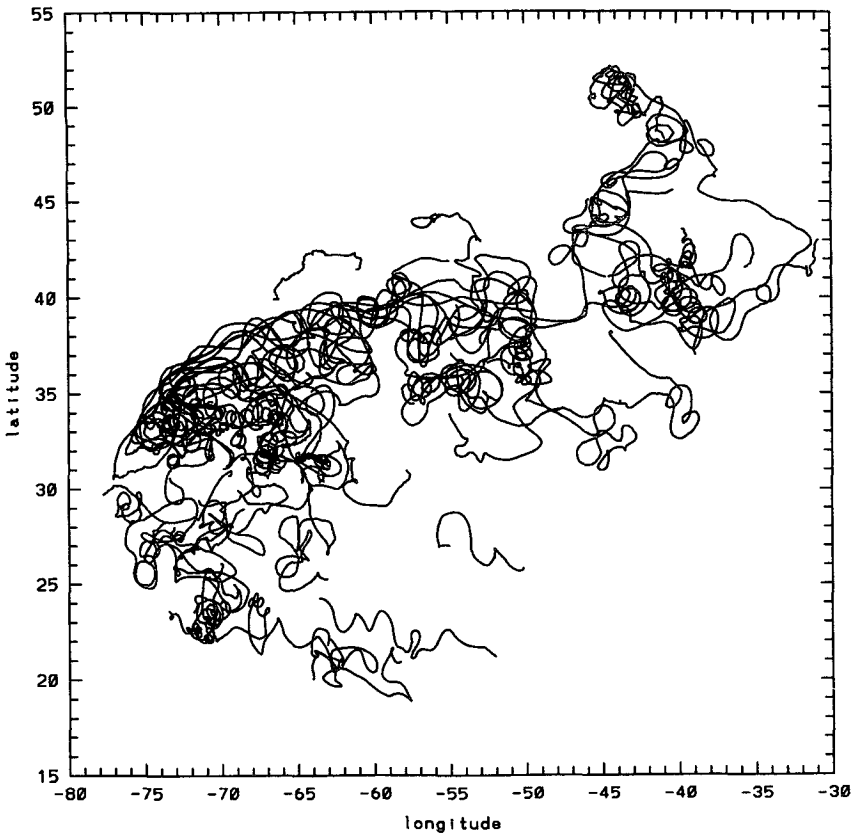

FIG. 1. The subset of "stationary" float trajectories.

some of the trajectories classified as stationary do have a significantly red low-frequency spectrum.

Power spectra of the total velocity time series have been computed for the stationary trajectories. As already mentioned by Owens (1991), the dataset exhibits quite a large variability. More specifically, we observe (i) a highly variable distribution of the energy content in the various frequency bands and (ii) a general absence of saturation at low frequencies. The actual number of floats, whose velocity spectra saturate at low frequencies, depends on the quantitative definition of saturation employed. We have opted to look at the relative variance of the three lowest frequency bands; by requiring the relative fluctuation of $P(\nu)$ to be less than 0.3 in these three frequency bands we find that only the 37% of the stationary trajectories satisfy the criterion.

Due to the high variability of the dataset, an unconditional averaging procedure will tend to mix very different behavior and scales. For this reason, we first identify the characteristics of the extreme behavior of the trajectories by using conditional averages on total energy spectra based on threshold values of the following parameters:

- a saturation parameter s defined as the relative fluctuation of the first three lowest frequencies
- the usual Lagrangian integral time T_L as defined by the rhs of (3)
- the relative percentage HF of kinetic energy in frequencies greater than $(10 \text{ days})^{-1}$.

This allows an identification of two extreme classes. These are

- CA1-type trajectories, characterized by saturation at low frequencies, a low energy content in the high frequencies ($HF < 0.05$), and $T_L > 5$ days
- CA2-type trajectories, characterized by a larger energy content in the high frequencies ($HF > 0.1$) and a smaller Lagrangian integral time $\frac{1}{2}P(\nu_{\min}) \sim T_L < 5$ days.

Clearly, the choice of the precise value of T_L for distinguishing between the two types of behavior is somewhat arbitrary, and it is difficult to assess the statistical significance of the results obtained with such small datasets. On the other hand, we note that the examination of the float trajectories of the two types (Figs. 2a and 2b) reveals quite different space and time characteristics. The 14 CA2 trajectories are clearly related to motions in highly energetic and coherent structures, such as meanders or isolated vortices, while the 9 CA1 trajectories are noticeably less energetic and

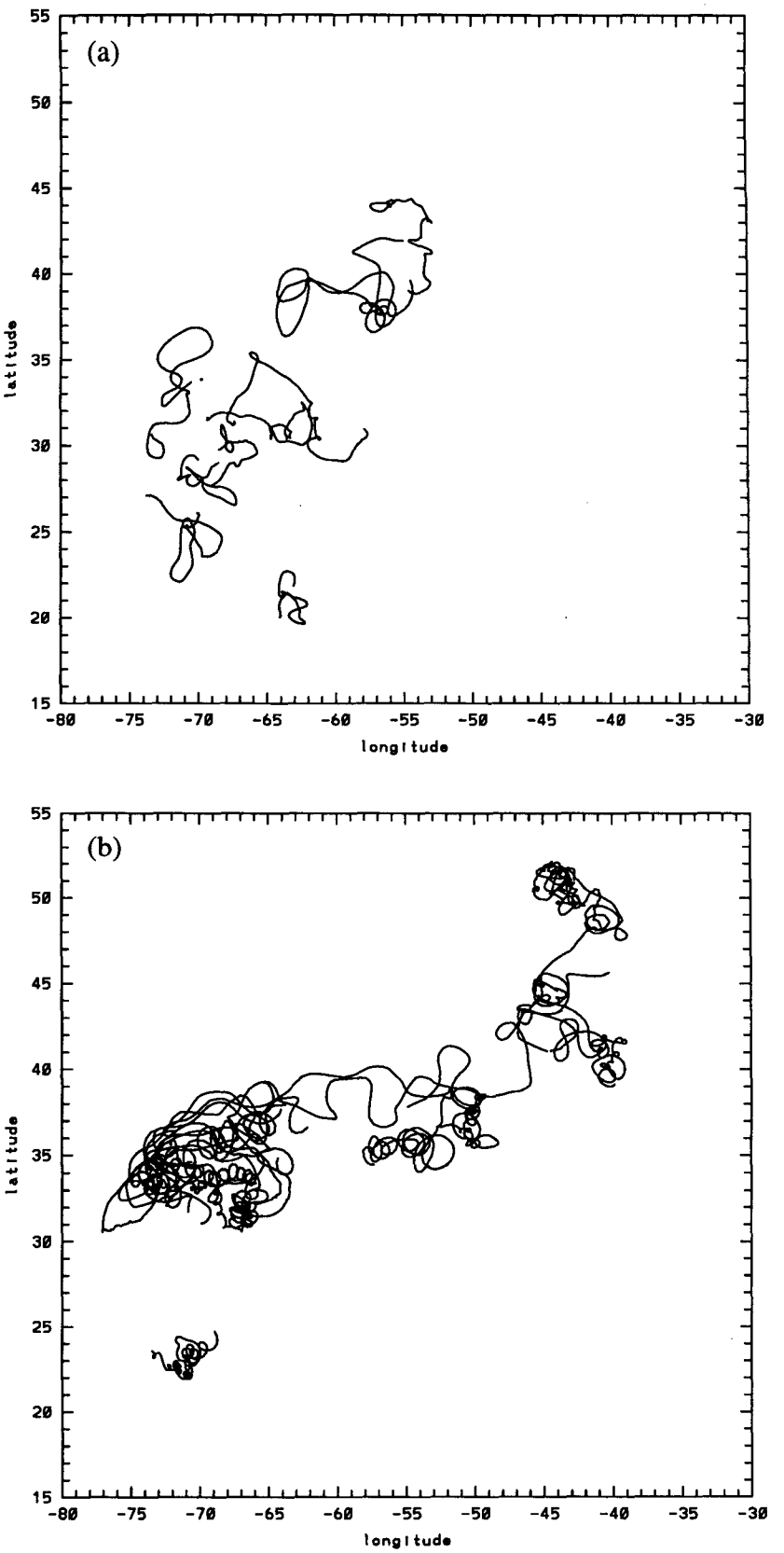

FIG. 2. (a) CA1 trajectories and (b) CA2 trajectories.

more typical of midocean conditions. The ordinates at the smallest frequency in Figs. 3a and 3b yield for the average value of T_L respectively 8 and 3 days for the CA1 and CA2 subsets, values that are well above and below the selected limiting value of 5 days. This indicates that the distinction between the two types of trajectories, although somewhat qualitative, does properly represent a different dynamical behavior.

Yet, the average velocity spectra of the trajectories corresponding to the two extreme types of behavior display some common features (Figs. 3a and 3b). Both spectra do, in fact, show a plateau in the low-frequency range and a steep spectral slope with $n > 3$ at larger frequencies, while at the largest frequencies resolved by the dataset, measurements errors induce a flattening of the spectrum (see appendix B). The most significant discrepancy between the two extreme spectra is observed at intermediate frequencies where the CA2-type spectrum displays an intermediate power-law regime with a slope of about 0.25, as indicated by the dotted line in Fig. 3b. As mentioned above, due to the way they were selected, the CA2 trajectories preferentially sample the high-energy regions close to coherent vortices. The existence of the intermediate spectral regime might thus be linked with the action of shear-dominated regions surrounding coherent structures, analogously to what has been observed in numerical simulations of two-dimensional turbulence (Elhmaidi et al. 1993 and section 5b).

Despite the high variability of the dataset, the existence of common features in the spectra of Figs. 3a and 3b motivates the search for a characteristic spectrum $P(\nu)$ that is representative of all stationary trajectories. Such a goal requires a rescaling of both the ordinate $P(\nu)$ and frequency axis ν by the appropriate dimensional timescale for each individual trajectory. Such a rescaling amounts to a nondimensionalization; the purpose is to take into account regimes of Lagrangian turbulence, with very different spatial and temporal scales, in order to reveal an eventual self-similar behavior.

An obvious candidate for rescaling both the ordinate $P(\nu)$ and the frequency ν axis is the usual Lagrangian integral timescale T_L [as defined by the rhs of Eq. (3)]. However, not all individual float spectra saturate at low frequencies, thereby disabling the use of (3) for all trajectories. This motivated us to introduce an alternative characteristic timescale T_L^*, which can be computed even for trajectories that do not exhibit a saturation at the lowest frequencies. Such a characteristic timescale T_L^*, which we can simply interpret as being the decorrelation timescale of a given trajectory, will enable us to compute a rescaled average spectrum for the stationary trajectories. We then pose

$$T_L = \mu T_L^*;$$

details of the actual methodology for computing T_L^* and μ are given in the next section.

3. An alternative method for computing T_L

Space and time decorrelation scales may be defined in both Eulerian and Lagrangian coordinates. In general, the link between the Lagrangian time and space decorrelation scales, T_L and L_L, and their Eulerian counterparts, T_E and L_E, may be quite complicated. Following Middleton (1985), we may infer this link in two simple extreme cases. Supposing the rms of velocity fluctuations σ_u to represent the typical scale of the turbulent velocities (square root of the eddy kinetic energy), the two extreme cases are characterized, respectively, by the assumptions (i) $T_E \ll L_E/\sigma_u$ and (ii) $T_E \gg L_E/\sigma_u$.

In the first case, the Lagrangian particles move slowly in the Eulerian field. Before the particles start exploring regions that are spatially decorrelated, the time decorrelation of the Eulerian field has already affected the particle motion. In this case, it is reasonable to expect the Lagrangian decorrelation time to be determined by the Eulerian decorrelation time, $T_L \approx T_E$. The lagrangian decorrelation length will also be determined by the Eulerian decorrelation time, $L_L \approx \sigma_u T_E \ll L_E$. This case corresponds to an Eulerian field, which is rapidly evolving on the advective timescale $T_{\text{adv}} = L_E/\sigma_u$.

Conversely, the second case corresponds to a field that is very slowly evolving (frozen field approximation) on the advective timescale T_{adv}. The Lagrangian decorrelation scale is now determined by the fact that the particles explore Eulerian regions that are spatially decorrelated. In this case, $L_L \approx L_E$, as the finite Lagrangian decorrelation length reflects the finite Eulerian space decorrelation. In this situation, $T_L \approx L_E/\sigma_u \ll T_E$.[1]

Using the equality sign $T_L = T_E$ or $L_L = L_E$ in the above expressions is rigorously possible only in the limit for respectively L_E or T_E going to zero. In both cases, $T_L \leqslant T_E$ and $L_L \leqslant L_E$. Under general circumstances, these unequalities have to be interpreted in an order of magnitude sense, indicating that the Lagrangian space and time decorrelation scales are expected to be not (much) larger than their Eulerian counterparts and that an adimensional constant of order one may enter the above formulas. In particular, we define a characteristic timescale $T_L^* = L_L/\sigma_u$, which may be derived from the above discussion in both the extreme cases, and it is related to the true Lagrangian decorrelation time by

$$T_L = \mu T_L^* = \mu \frac{L_L}{\sigma_u}, \tag{5}$$

where μ is a constant proportionality factor.

[1] Oceanic mesoscale turbulence is more likely to be closer to this second limit of almost frozen field approximation since we have seen that Lagrangian spectra present slopes steeper than 3 at high frequencies.

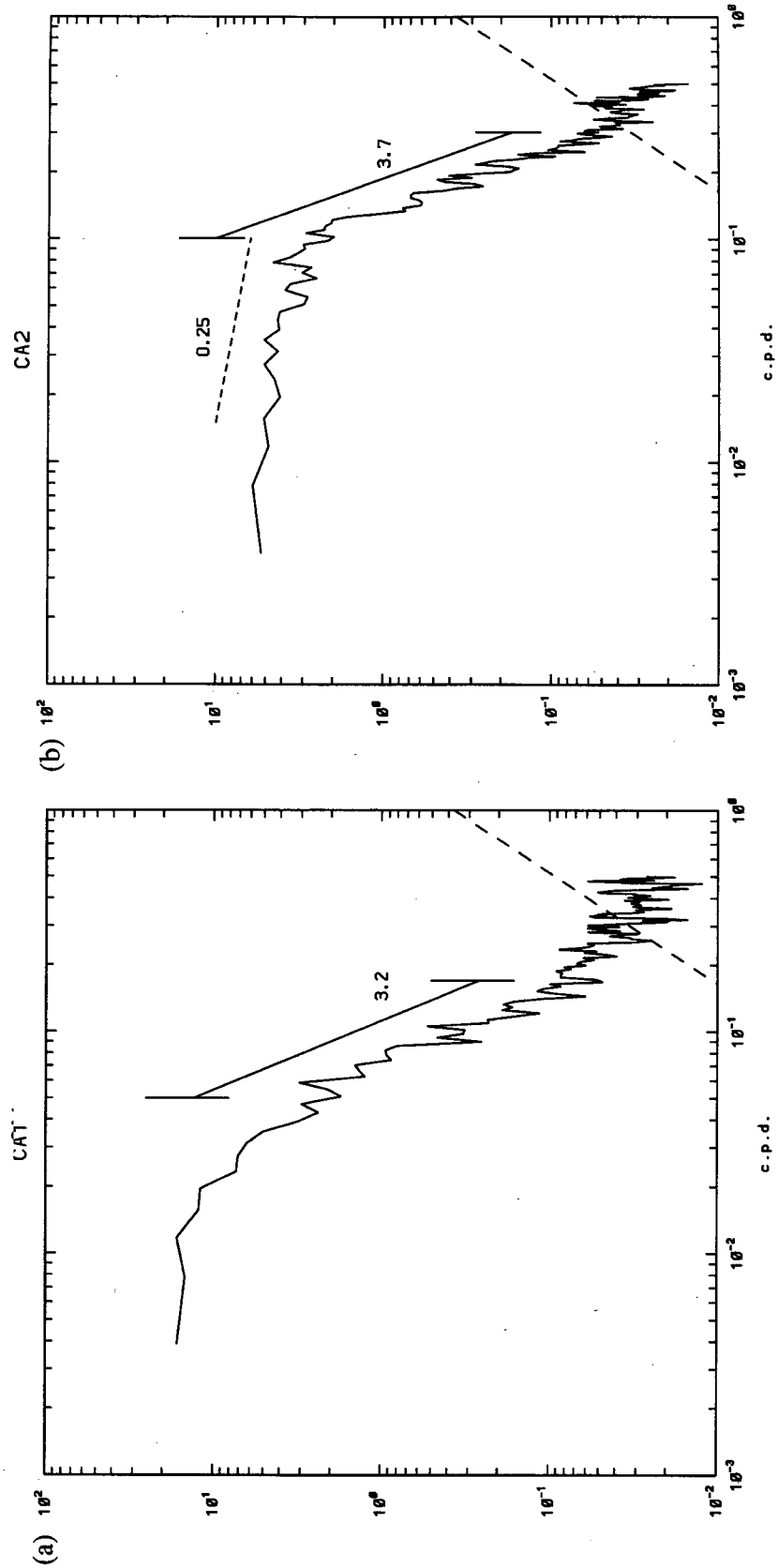

FIG. 3. Total energy spectrum of (a) the CA1 subset and (b) the CA2 subset. The dashed line at high frequencies indicates the error estimate in kinetic energy due to errors in position tracking. The error bars indicate the 90% confidence interval computed using the χ^2 test. Units on the ordinate axis are given in days.

Operationally, the constant μ is determined in such a way that the value of T_L defined by (5) coincides on average with the rhs of (3) for those specific trajectories that saturate at low frequencies and for which relation (3) is valid. This coincidence, however, is true only on average; moreover, μ depends on the quantitative choice for the definition of saturation. To give an idea of the range of variation of μ, when we choose the saturation parameter s between 0.1 and 0.3, we find that between 8 and 26 float trajectories saturate, and values of $\bar{\mu}$ belong to the interval $0.57 < \bar{\mu} < 0.67$. When we consider only trajectories of the CA1 subset, we obtain $\bar{\mu} = 0.6$. In practice, we choose $\mu = 0.6$ to estimate T_L from (5) and for producing the nondimensional average spectrum of Fig. 5a (see next section). We have also performed a sensitivity test of the average spectrum on the actual choice of μ in its interval of variability and found no significant influence.

As for the determination of the spatial decorrelation length L_L, we resort to a method that is commonly used for studies of fractal properties of trajectories (e.g., Osborne et al. 1986, 1989; Provenzale et al. 1991). It consists in measuring the length of the float trajectory as a function of a variable yardstick segment Δ and by approximating the curve with a broken line whose individual segments have length Δ. Operationally, one starts from the first point $\mathbf{x}(t_0)$ of the trajectory and looks for the point $\mathbf{x}(t_{i_1})$ such that $|\mathbf{x}(t_{i_1}) - \mathbf{x}(t_0)| \approx \Delta$, this defines the index i_1. Then the procedure is repeated starting from $\mathbf{x}(t_{i_1})$, looking for a point $\mathbf{x}(t_{i_2})$ such that $|\mathbf{x}(t_{i_2}) - \mathbf{x}(t_{i_1})| \approx \Delta$, and so on. This allows for defining a set of indices i_n, $n = 1, \cdots, N(\Delta)$, which label the vertices of the broken line approximating the real trajectory. The length of the trajectory is then approximated by

$$L(\Delta) = \sum_{n=1}^{N(\Delta)} [(\mathbf{x}(t_{i_{(n+1)}}) - \mathbf{x}(t_{i_n}))^2]^{1/2} \approx \Delta N(\Delta). \tag{6}$$

The dependence of i_n on the index n is a complicated function that depends on the geometry and complexity of the trajectory.

On average, $L(\Delta)$ is a nonincreasing function of Δ. An eventual power-law behavior of $L(\Delta)$ can be related to a fractal behavior of the trajectory, the fractal dimension D_L of the trajectory being in this case defined by the expression:

$$L(\Delta) \propto \Delta^{1-D_L}. \tag{7}$$

For mathematical fractal curves, the fractal behavior extends to infinitesimally small scales and the length $L(\Delta)$ is really divergent. For physical fractal curves, on the other hand, the requirement of differentiability at the smallest scales induces a convergence of the length $L(\Delta)$ to a finite value $L(0)$, and the power-law behavior (7) is eventually observed on a finite range of scales (Isichenko 1992).

In this case, the behavior of $L(\Delta)$ for small Δ involves the notion of decorrelation length L_L, and one can define L_L such that

$$L(L_L) = pL(0). \tag{8}$$

An interpretation of the above definition is that the Lagrangian velocity along the trajectory remains correlated for scales smaller than the decorrelation length, and the constant p defines the degree of correlation of $L(\Delta)$ when integrated over a decorrelation length. This definition of L_L is simply a space analogue of a decorrelation time based on a velocity correlation function.

Figure 4 show the plot of $L(\Delta)$ versus Δ for three typical example trajectories; the corresponding values of L_L are indicated. The paths of floats B59 and B79 are prototypical examples of trajectories dominated by a single length scale; they have been chosen to illustrate the meaning of L_L. For float B59, in particular, $L(\Delta)$ displays an abrupt decrease or "jump" for a yardstick length of the order of the characteristic length scale (i.e., $\Delta = L_L \sim 70$ km). This value $L_L \sim 70$ km closely corresponds to the scale that may be determined by a "visual" inspection of the trajectory and it corresponds to $p = 0.7$ in (8). On the other hand, float B17 is an example of a trajectory that exhibits several length scales; in this case, $L(\Delta)$ is less steep. Expressions (8) and (5) with $\mu = 0.6$ and $p = 0.7$ allow us to obtain an estimate of T_L for every float. As for μ, the precise value chosen for p is not critical.

4. A generic Lagrangian spectrum shape

Having obtained an estimate of T_L for each individual trajectory, we compute the nondimensional quantities

$$\hat{\nu} = \nu T_L \quad \hat{P}(\hat{\nu}) = P(\nu T_L)(T_L)^{-1} \quad (\hat{t}) = t(T_L)^{-1}.$$

Note that with this normalization the asymptotic value of $\hat{P}(\hat{\nu})$ for $\hat{\nu} \to 0$ is equal to 2 for floats whose spectrum saturates at low frequencies. The average nondimensional spectrum for all trajectories is represented by the continuous curve of Fig. 5a. There is clearly a generic spectrum shape, characterized by a flat plateau extending up to $\nu_0 \sim (30T_L)^{-1}$, a steep decrease for $\nu \geqslant \nu_1 = (3 \sim 4\ T_L)^{-1}$ characterized by a slope $n = 3.3 \pm 0.14$ (see Table 1), and an intermediate regime for $\nu_0 \leqslant \nu \leqslant \nu_1$ that displays a power law behavior with a slope $\alpha = 0.25 \pm 0.06$. The values ν_0, ν_1, n, and α have been obtained by least square fits to the spectral shape of Fig. 5a while taking into account the constraints (1) and (3). The indicated uncertainties on the slopes are the 95% confidence limit of the least square fits.

The average spectrum shape (Fig. 5a), representative of all 56 stationary trajectories, displays characteristics that are dominated by CA2 characteristics in the intermediate and low frequency bands, while it is closer to the spectrum of CA1 in the high frequency band

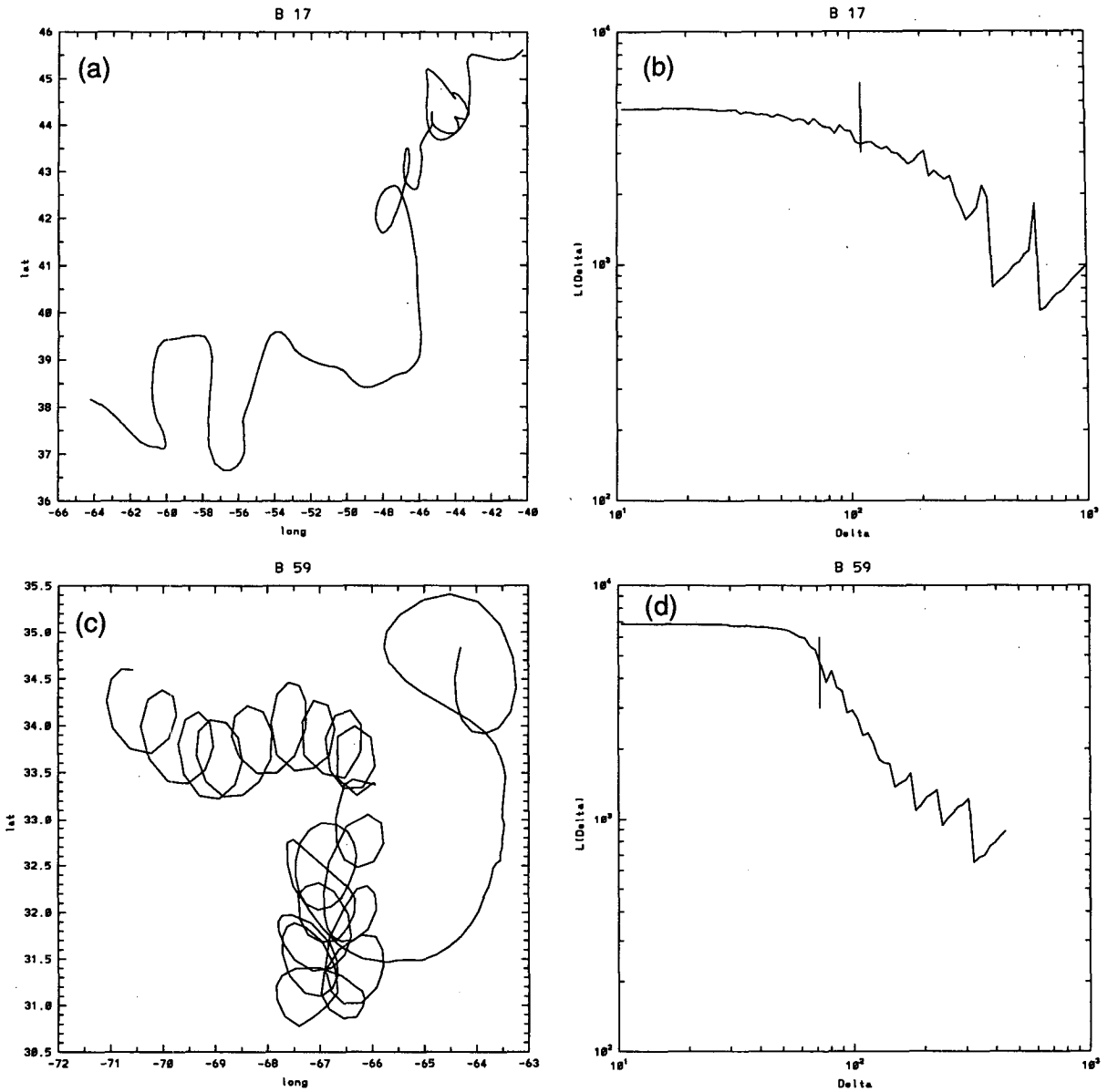

FIG. 4. Panels (a), (c), and (e) show three example trajectories; panels (b), (d), and (f) show the corresponding length $L(\Delta)$ as measured by the yardstick method. Units of $L(\Delta)$ and Δ are in kilometers. The value of the decorrelation length L_L is indicated by the position of the vertical line in (b), (d), and (f).

(Figs. 3a and 3b). In particular, the value of the slope $n = 3.3$ in the high frequency band is very close to the value of $n = 3.2$ for the CA1 subset. It is thus of interest to discuss the quantitative influence of the 9 CA1 and 14 CA2 trajectories on this average spectrum. The respective values of T_L for CA1 and CA2 are about 8 and 3 days (section 2). These values of T_L imply that the nondimensionalization of the frequency axis yields a stronger weighting of the CA1 subset for the high values of $\hat{\nu}$. Conversely the CA2 subset, which has a shorter T_L, has a stronger weighting in the lowest and intermediate frequency bands. The presence of the power-law regime $P(\nu) \propto \nu^{-0.25}$ in the average velocity spectrum of Fig. 5a confirms the dominance of the CA2-type behavior in the frequency band $\nu_0 \leqslant \nu \leqslant \nu_1$. We have noted in section 2 that the existence of this intermediate power-law regime corresponds to the trajectories that explore energetic persistent structures such as coherent structures and jet meanders. Finally, as already observed for the CA1 and CA2 types, the highest frequencies $\hat{\nu} \geqslant 1$ in the dataset are dominated by measurement errors and have been truncated. It is

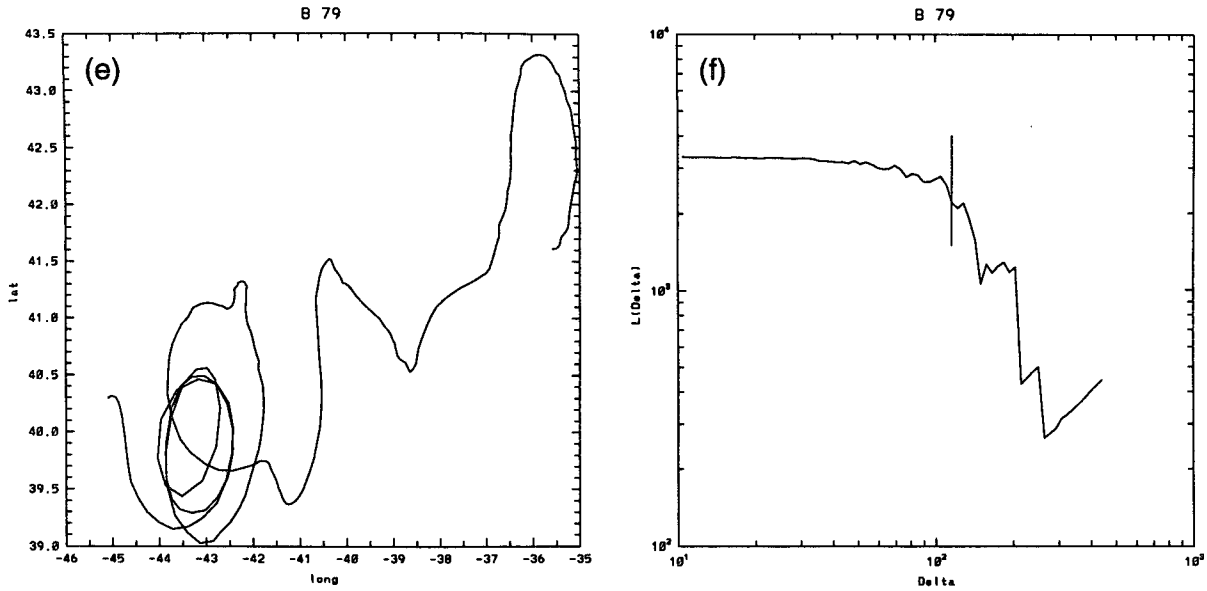

FIG. 4. (*Continued*)

unclear to us what the maximal frequency limit of this steep slope range is in reality.

The generic shape suggested by the continuous line of Fig. 5a is further supported by results on Lagrangian geostrophic turbulence simulations (Hua and McWilliams 1994, manuscript submitted to *J. Fluid Mech.*), where Lagrangian velocity spectra are computed from the numerical trajectories of 1024 particles launched in a stratified stationary geostrophic turbulent flow on the β plane. The results of the direct numerical simulations (DNS) (Fig. 5b, continuous line) also indicate that beyond the low-frequency plateau, the spectrum displays an intermediate power-law regime $\nu^{-\tilde{\alpha}}$ for $\tilde{\nu}_0 \leqslant \nu \leqslant \tilde{\nu}_1$ and a steep slope $\tilde{n}$ for $\nu \geqslant \tilde{\nu}_1$ up to frequencies close to numerical noise frequency, at $\nu \sim \nu_f$, where ν_f is determined by the hyperviscosity of the numerical model, which is necessary for handling the enstrophy cascade at the smallest spatial scales. Least square fits to the numerical spectrum provide $\tilde{\nu}_0 \sim \nu_0$, $\tilde{\nu}_1 \sim \nu_1$, and $\tilde{\alpha} \sim \alpha$. Note however that the DNS example of Fig. 5b presents substantially steeper slopes at very high frequencies ($\tilde{n} \geqslant 5$) than in the northwest Atlantic data. The DNS further reveal that this slope, which is always larger than 3, is sensitive to the degree of intermittency of the turbulence (i.e., the existence of strong coherent vortices). However, if we limit the least square fit to the frequency range that is correctly sampled by the data (i.e., $\nu T_L < 1$), we get $\tilde{n} \sim n$.

That the generic velocity spectrum of the stationary 700-m floats displays a slope steeper than 3 at large frequencies implies that the power spectrum $W(\nu)$ of Lagrangian acceleration

$$W(\nu) \propto \nu^2 P(\nu)$$

is integrable and that the variance of the acceleration is finite. In other words, the quantity

$$\frac{\mathbf{u}(t + \Delta t) - \mathbf{u}(t)}{\Delta t}$$

converges in the mean-square sense toward the acceleration $\mathbf{a}(t)$ and

$$\frac{d}{dt}\mathbf{u}(t) = \mathbf{a}(t) = \lim_{\Delta t \to 0} \frac{\mathbf{u}(t + \Delta t) - \mathbf{u}(t)}{\Delta t}$$

is well defined in a statistical sense (Panchev 1971) and is continuous. It is worth emphasizing that a finite value of the variance of the acceleration supports a truly "Lagrangian" behavior of the 700-m floats even for an infinite extent of the inertial range. This type of behavior is different with respect to that considered by various stochastic models of particle trajectories (e.g., see Griffa et al. 1995), which rely upon discontinuous Lagrangian accelerations.

5. Contributions of the different spectral bands to dispersion

This section is devoted to the study of the structure function of the (linearly detrended) Lagrangian position $\mathbf{x}'(t)$, given by

$$S(\tau) = \langle [\mathbf{x}'(t + \tau) - \mathbf{x}'(t)]^2 \rangle. \qquad (9)$$

The aim is to identify the role of the different spectral frequency bands in determining the form of the struc-

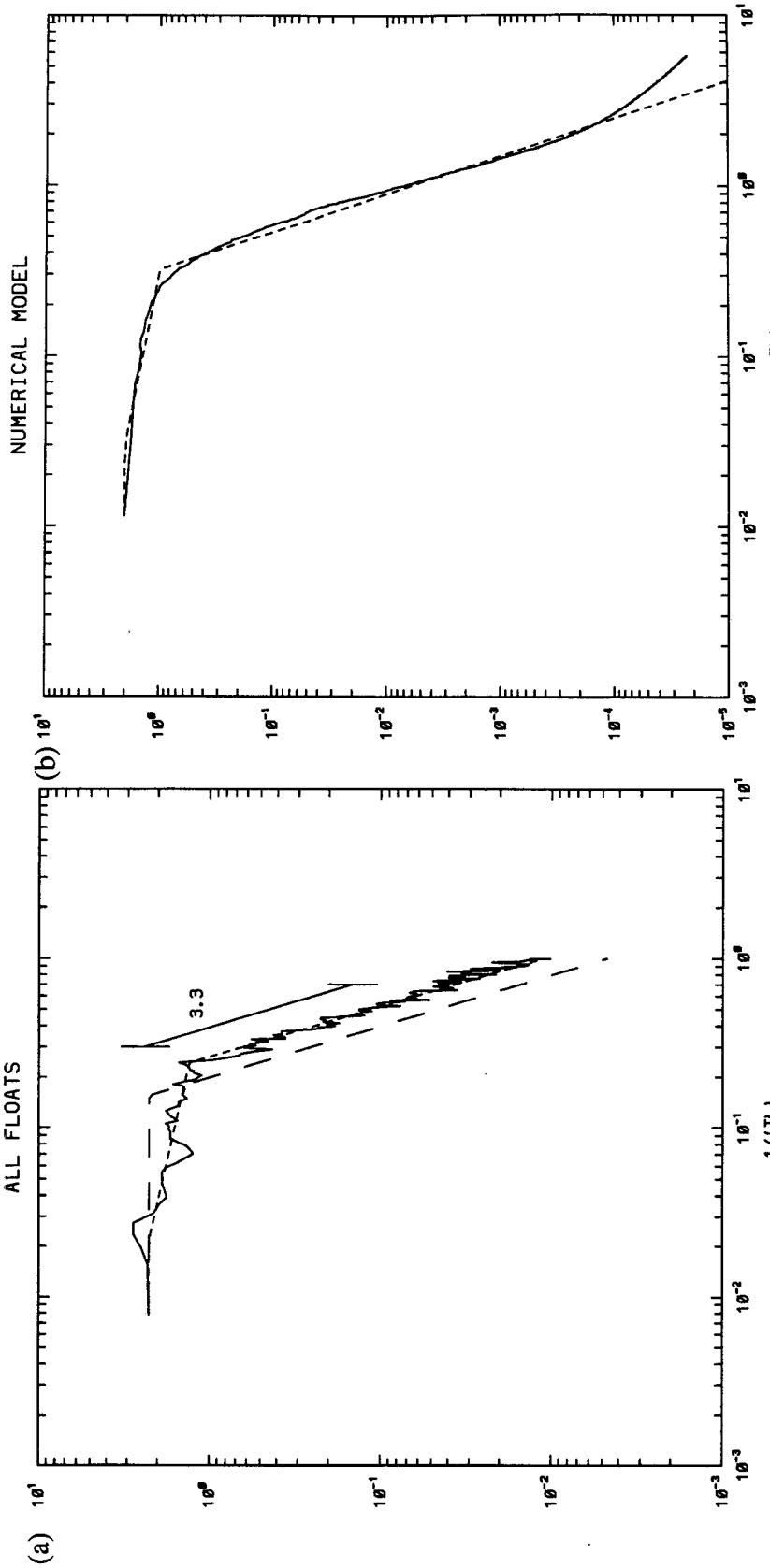

FIG. 5. (a) Rescaled total energy spectrum of the 56 stationary trajectories. The frequency is normalized by T_L^*, where T_L^* is defined in section 3. The error bars indicate the 90% confidence interval computed using the χ^2 test. (b) Total energy spectrum from the numerical simulation of 1024 Lagrangian trajectories in a stratified geotrophic turbulent flow on the β-plane (from Hua and McWilliams 1994). The dashed line in Fig. 4a corresponds to a two-piece fit (section 4a) and the dotted lines in Figs. 4a and 4b correspond to a three-piece spectral fit (see section 4b).

TABLE 1. Logarithmic spectral slopes and number of points N used to estimate the slope for the normalized spectra of the floats. The indicated uncertainties are the 95% confidence limits to the least square fit to the spectrum in the selected frequency range.

Slope	$\Delta\nu' (T_L)^{-1}$	N
$n = 3.3 \pm 0.14$	0.3–0.7	70
$\alpha = 0.25 \pm 0.06$	0.025–0.25	41

ture function (and therefore the dispersion[2]) and to draw the dynamical implications of the generic spectral shape identified in the previous section.

Following the normalization introduced earlier, we define a nondimensional structure function $\hat{S}(\hat{\tau})$, which is related to the total energy spectrum by

$$\hat{S}(\hat{\tau}) = \frac{S(\tau)}{\sigma_u^2 T_L^2} = \frac{8}{4\pi^2}\int_0^\infty \frac{\hat{P}(\hat{\nu})}{\hat{\nu}^2}\sin^2(2\pi\hat{\nu}t/2)d\hat{\nu}, \quad (10)$$

where the frequency $\hat{\nu}$ and spectrum $\hat{P}(\hat{\nu})$ are the nondimensional quantities defined in section 2. In particular, we have

$$\hat{P}(0) = 2$$
$$\int_0^\infty \hat{P}d\hat{\nu} = \frac{1}{2}.$$

For simplicity, from now on we drop the caret to indicate nondimensional quantities. In the following we investigate two simple analytical approximations to the Lagrangian spectrum, obtained by using a piecewise power-law spectrum with respectively two and three pieces.

a. *Two-piece fit*

The shape of the average Lagrangian spectrum measured in situ (continuous line in Fig. 5a) suggests a first analytical representation of the form

$$P_a(\nu) = P_1(\nu) + P_2(\nu) = 2\left[H(\nu_1) + \left(\frac{\nu_1}{\nu}\right)^n (1 - H(\nu_1))\right], \quad (11)$$

where $H(\nu_1) = 1$ for $\nu < \nu_1$ and 0 elsewhere. The spectrum is the sum of two contributions P_1 and P_2, which represent the low and high frequency branches of the dashed line in Fig. 5a. These two parts of the spectrum are idealizations of the low-frequency plateau and the steep spectral decrease at large frequencies. The slope n represents the slope of the high-frequency part of the spectrum; we want to quantify the impact of various values of n on the behavior of the Lagrangian structure function.

By equating the areas beneath the continuous and dashed curves of Fig. 5a, we conserve the total variance through

$$\nu_1 = \frac{n-1}{n}\frac{1}{4}. \quad (12)$$

Relations (11) and (10) enable us to quantify the respective role of P_1 and P_2 in shaping the structure function of the Lagrangian position. The corresponding analytical approximation to the structure function,

$$S_a(\tau) = S_1(\tau) + S_2(\tau), \quad (13)$$

is the sum of the respective contributions of the low and high frequency bands. The functions $S_a(\tau)$, $S_1(\tau)$, and $S_2(\tau)$ are plotted in Figs. 6a and 6b for $n = 2$ and $n = 3.3$ respectively. The latter value of n corresponds to the average slope obtained for the total energy spectrum of the stationary trajectories (see Table 1 and Fig. 5a). Figure 6 indicate that the low frequency band contributes to the structure function much more than the high frequency band for both values of n. Moreover, using (10), (11), and (12), we get

$$\lim_{\tau\to 0}\frac{S_1(\tau)}{S_2(\tau)} = n - 1. \quad (14)$$

Therefore, provided that the decrease at large frequencies is steep enough, the dominance of the low frequency band holds even for the shortest time lags of the structure function. In particular, for $n \geq 3$ more than 66% of the energy content is in $P_1(\nu)$ and $S_1(\tau) > S_2(\tau)$ for all τ.

For $n = 3.3$, corresponding to the in situ observations (Fig. 6b), the low-frequency contribution $S_1(\tau)$ is always significantly much larger than $S_2(\tau)$, by almost an order of magnitude, for all time lags. All the characteristic features of the structure function, such as the short time "ballistic" τ^2 regime and the large time "Brownian" τ regime, as well as the transition region between them, are predominantly determined by the low-frequency motions. For the case of a two-piece fit, the transition between the τ^2 and τ regimes occurs at about $\tau = 2 \sim 3\ T_L$; for values of $n > 2$, the transition between the two regimes is found to be only weakly dependent on n.

b. *Three-piece fit*

We want now to better study the transition between the τ^2 and τ regimes of the structure function by resorting to a three-piece fit of the spectrum. This corresponds to the dotted line of Figs. 5a and 5b, which is of the form

[2] We recall that the diffusion coefficient is usually defined as $\frac{1}{2}(d/d\tau)S(\tau)$.

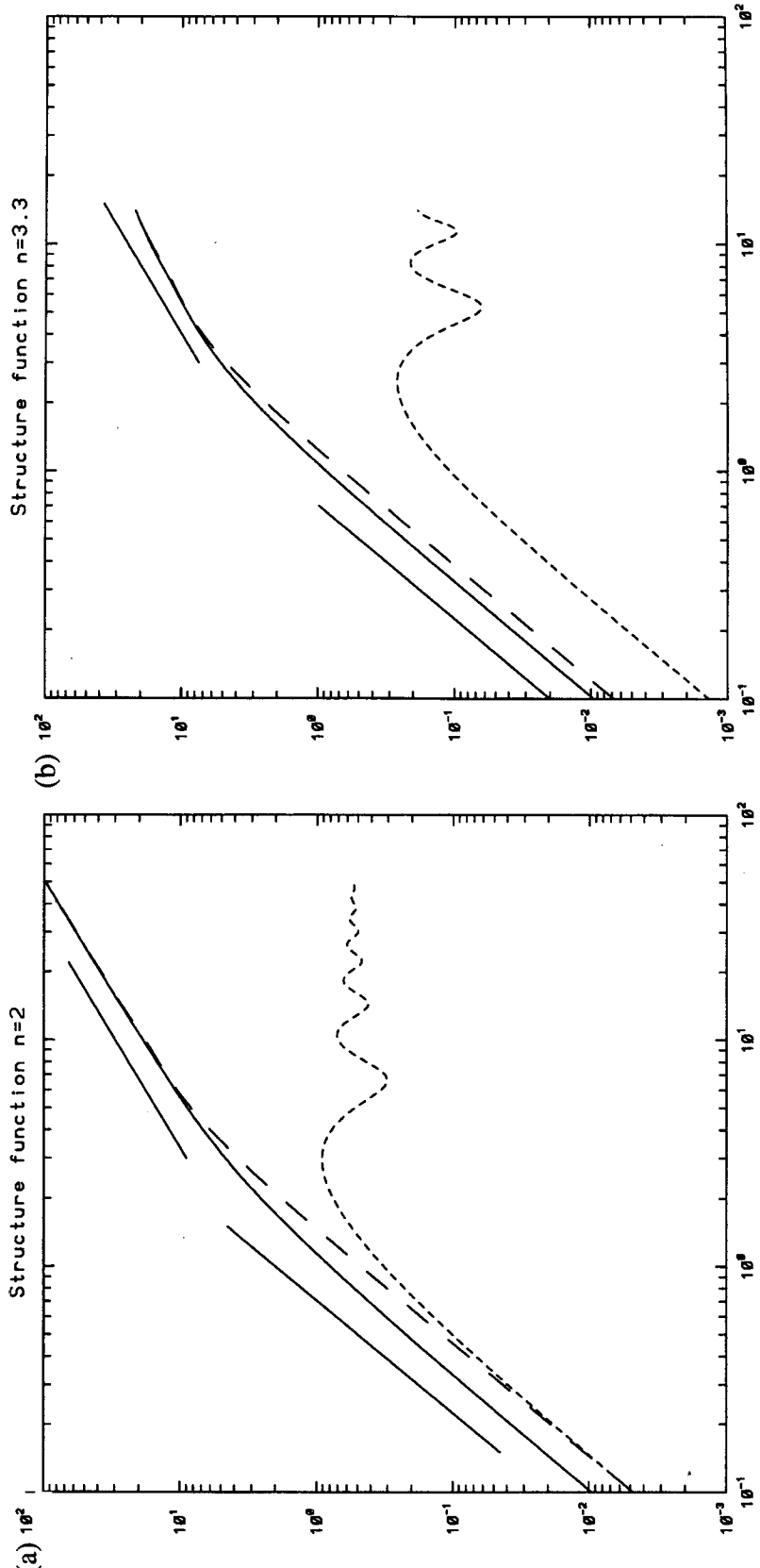

FIG. 6. (a), (b). Structure functions of Lagrangian position for, respectively, $n = 2$ and $n = 3.3$. The total structure function $S_n(\tau)$ is indicated by the continuous line, $S_1(\tau)$ by the dashed line, and $S_2(\tau)$ by the dotted line. The two full straight lines represent the two asymptotic regimes $S(\tau) \propto \tau^2$ and $S(\tau) \propto \tau$.

$$P_a(\nu) = 2\left[H(\nu_0) + \left(\frac{\nu_0}{\nu}\right)^{\alpha} I(\nu_0, \nu_1) + \left(\frac{\nu_0}{\nu_1}\right)^{\alpha}\left(\frac{\nu_1}{\nu}\right)^{n}(1 - H(\nu_1))\right], \quad (15)$$

where $I(\nu_0, \nu_1) = 1$ for $\nu_0 < \nu < \nu_1$ and 0 elsewhere.

Figure 7a shows the compensated structure functions $S(\tau) \times \tau^{-1}$, as computed respectively from the in situ data (continuous line), the two-piece spectrum (dashed line), and the three-piece spectrum (dotted line). The compensation by τ^{-1} has been performed in order to better display the intermediate and Brownian regimes in the log–log plot. Figure 7a clearly shows that the three-piece fit yields a significantly better approximation to the observed structure function than the two-piece fit. In particular, the three-piece fit enables a better representation of the intermediate regime of

$$1 < \frac{\tau}{T_L} < 10,$$

where there is a tendency for an extended power-law behavior, and the Brownian regime in τ does not start until $\tau \approx 10T_L$. This delay of the Brownian regime when compared to the two-piece fit and the existence of an intermediate extended power-law behavior are reminiscent of the findings of Elhmaidi et al. (1993). These authors have documented the anomalous diffusion at intermediate times caused by the existence of persistent coherent vortices in simulations of two-dimensional turbulence. The trapping of particles by long-lived structures causes a delay in the transition to the Brownian dispersion, generating an intermediate anomalous dispersion regime, bounded at large times for spatially homogeneous turbulence.

Figure 7b shows the various contributions to the total structure function (continuous line) for the three-piece fit; the dotted, short-dashed, and dashed lines correspond respectively to the lowest, intermediate, and highest frequencies. We note that at all time lags, the largest contribution comes from the intermediate frequencies; again, the highest frequencies provide a negligible contribution. The Brownian regime is determined by both the intermediate and lowest frequencies, while the intermediate regime, which corresponds to

$$1 < \frac{\tau}{T_L} < 10,$$

is solely determined by the second piece of the three-piece fit. We have therefore provided evidence for a close correspondence between the existence of an intermediate power-law regime in the spectrum and an intermediate regime in the behavior of the structure function (and thus in the absolute dispersion). We have already noted in section 2 that the existence of this intermediate regime in the spectrum is characteristic of the CA2 trajectories, which preferentially sample high-energy regions close to coherent vortices and strong jets.

6. Discussion and conclusions

This paper shows that, pending an appropriate scaling of each trajectory by its Lagrangian integral timescale T_L, there exists a generic shape of Lagrangian frequency spectrum for "stationary" trajectories in the western North Atlantic. Such a rescaling requires to estimate the value of T_L for each trajectory; we have proposed an alternative methodology based on an average proportionality between T_L and a decorrelation timescale T_L^*, which can be deduced through dimensional considerations from a yardstick measure of the Lagrangian decorrelation length L_L.

The generic spectral shape consists in a plateau at the lowest frequencies extending up to $\nu_0 \sim (30T_L)^{-1}$, an intermediate slope with $\alpha = 0.25$ between ν_0 and $\nu_1(3 \sim 4\ T_L)^{-1}$, and a steep slope $n \geq 3$ at larger frequencies. Such a steep slope at large frequencies implies that most of Lagrangian dispersion can be ascribed to low and intermediate frequency motions. The predominance of low frequency on dispersion requires in fact the high frequency to be slope $n \geq 2$. A stronger result, which requires $n \geq 3$, is that the spectrum shape is compatible with continuous material particle accelerations and finite variance of the Lagrangian accelerations (section 4). This case supports a truly "Lagrangian" behavior of the 700-m floats even for an infinite extent of the inertial range.

We have provided some evidence from the data and from a three-piece linear fit of the Lagrangian spectrum that the observed delay of the Taylor–Brownian regime, which is reached in the data only for time lags larger than $10T_L$, can be ascribed to the existence of an intermediate power-law regime in the spectrum. This intermediate regime is characteristic of floats sampling energetic persistent features, such as strong jets and/or coherent vortices, while it does not appear to exist for less energetic midocean trajectories.

We recall that in past years some attention has been devoted to the study of anomalous dispersion and fractal behavior of both surface drifter and SOFAR float trajectories (Osborne et al. 1986, 1989; Brown and Smith 1990; Provenzale et al. 1991; Sanderson and Booth 1991). In particular, for surface drifters the analysis of Osborne et al. (1986, 1989), has indicated the existence of an intermediate spectral slope with $\alpha' \approx 0.6$, associated with an anomalous dispersion law $S(\tau) \propto \tau^{5/3}$ in the structure function. In their study of absolute dispersion in 2D turbulence, Elhmaidi et al. (1993) have detected both a $t^{5/4}$ and a $t^{5/3}$ law for the ensemble dispersion of advected tracers. The former was shown to be associated with particle motion in proximity of coherent vortices and it is analogous to the intermediate regime observed in the spectrum of the CA2-type SOFAR float trajectories. The $t^{5/3}$ dis-

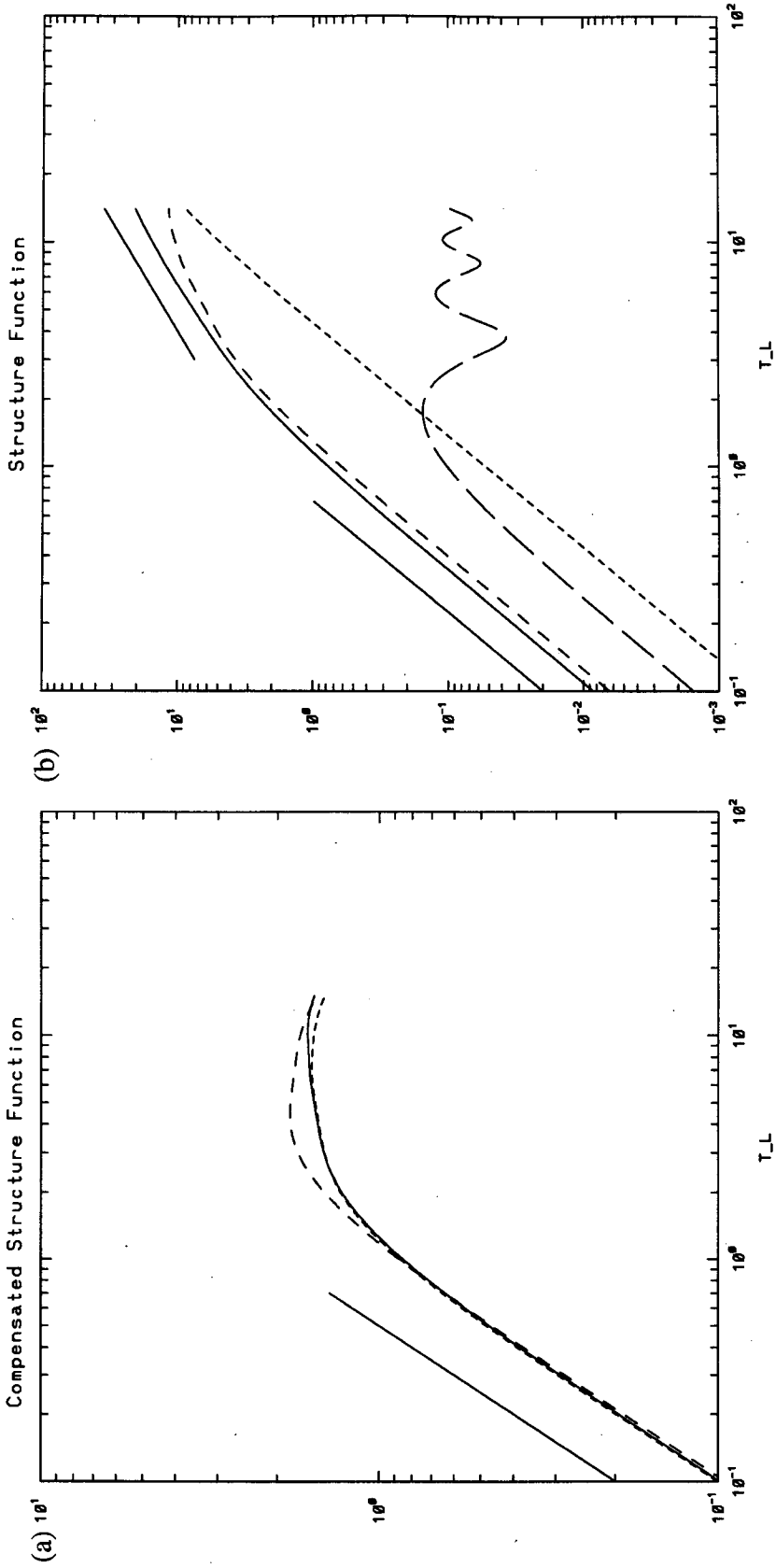

FIG. 7. (a) Compensated structure functions for the float data (continuous line), for a two-piece spectral fit (dashed line) and for the three-piece fit (dotted line). The structure function has been compensated by τ^{-1}. The full straight line represents the asymptotic regime τ^{-1}. $S(\tau) \propto \tau$. (b) Total structure function (continuous line), together with the contribution from the lowest (dotted line), intermediate (short-dashed line), and highest (dashed line) frequency bands for the three-piece spectral fit. The two full straight lines represent the two asymptotic regimes $S(\tau) \propto \tau^2$ and $S(\tau) \propto \tau$.

persion law, on the other hand, was shown to be related to the motion of vorticity-dominated, incoherent patches in the background between the vortices. We note the analogy between the values found by Osborne et al. (1986, 1989) for surface drifters and those obtained for the vorticity-dominated patches in 2D turbulence. Due to the discontinuous particle accelerations observed for surface drifters, however, it still remains to be assessed whether surface motions may be interpreted in terms of 2D dynamics and compared with the results found for the truly quasigeostrophic dynamics of SOFAR floats.

We also note that Middleton (1985) has developed the argument that steep Lagrangian spectra are to be expected if the Eulerian wavenumber spectra are themselves steep. This is supported by DNS of quasigeostrophic turbulence (e.g. Hua and Haidvogel 1986), where Eulerian wavenumber spectra are steeper than k^{-4}. Furthermore, we have noted a close analogy between the rescaled average spectrum measured in situ and the Lagrangian spectra computed in DNS of quasigeostrophic turbulence (Hua and McWilliams 1994, manuscript submitted to *J. Fluid Mech.*).

A side issue of this work concerns the contrast between the Lagrangian velocity spectrum slopes and the observed ν^{-2} Eulerian ones (Wunsch 1982), with a steeper slope prevailing for the Lagrangian case. This result is dynamically compatible with the common in situ observation that the Lagrangian integral timescale is shorter than its Eulerian counterpart; this behavior is confirmed by the DNS of Hua and McWilliams (1994, manuscript submitted to *J. Fluid Mech.*).

As a concluding remark, we note that the analysis of the North Atlantic SOFAR floats datasets at 700 meters has indicated both the existence of apparently generic features in the behavior of Lagrangian quantities as well as intriguing similarities between field observations and numerical simulations of quasigeostrophic flows for trajectories that are stationary on the timescale of 200 days. On the other hand, both the statistical significance of these results and their applicability to other flow conditions remain to be fully explored. We leave this to further investigation.

Acknowledgments. We would like to thank B. Owens for generously providing us with the Lagrangian historical dataset in the northwestern Atlantic. Comments on the manuscript by Dr. Klein are gratefully acknowledged.

APPENDIX A

Stationarity of Velocity Time Series

Given a generic time series $\xi(t)$, we say that it has stationary average if its mean

$$\bar{\xi}(t_0, \tau) = \frac{1}{2\tau} \int_{t_0-\tau}^{t_0+\tau} \xi(t)dt$$

is independent of both t_0 and τ for sufficiently large values of τ.

In the case of float trajectories, we consider the scalar time series of position $x(t)$ and velocity $v(t) = dx/dt$, and we want to verify whether the velocity time series has a stationary average, that is, if there is no net Lagrangian acceleration. To this end, we consider the linear least-square fit $v_{ls}(t) = \gamma t + c$ to $v(t)$, and we rewrite the two series as

$$\begin{cases} x(t) = x'(t) + ct + \frac{1}{2}\gamma t^2 \\ v(t) = v'(t) + c + \gamma t, \end{cases}$$

where now $x'(t)$ and $v'(t)$ are stationary and the quantity γ represents the net Lagrangian acceleration. Note that the presence of a trend in a velocity time series with total length T is related to the presence of significant components with periodicity *longer* than T. Clearly signals which are nonstationary on the timescale T may well become stationary on much longer timescales.

A common procedure when studying Lagrangian float trajectories is to linearly detrend the position time series in order to eliminate a constant mean advection velocity (e.g., Provenzale et al. 1991). In the above case, the linearly detrended position time series is

$$\tilde{x}(t) = x(t) - \kappa t = x'(t) + (c - \kappa)t + \frac{1}{2}\gamma t^2,$$

where $\kappa = c + \frac{1}{2}\gamma T$ is the mean slope of the linear least-square fit to the position time series of length T. If $\gamma = 0$ (i.e., the velocity time series is stationary as there is no net Lagrangian acceleration), linearly detrending $x(t)$ gives $\tilde{x}(t) = x'(t)$, providing the correct signal. In this case the velocity $v(t)$ is (apart from the constant $v_{ave} = c$ that may be easily eliminated) the derivative of $\tilde{x}(t)$. When $\gamma \neq 0$, however, linearly detrending $x(t)$ may be inappropriate since the mean velocity itself is not constant in time and $v(t) - c$ is not the derivative of $\tilde{x}(t)$.

We now want to have a simple operational way for determining whether the velocity time series is stationary. A first possibility is to perform a linear least-square fit to $v(t)$ in order to determine the value of γ. This may be troublesome, however, due to the large uncertainties in $v(t)$ when the velocity is obtained by numerical differentiation of $x(t)$ and to the possible presence of higher-order trends in $x(t)$. Alternatively, we may follow the simple procedure of comparing the power spectra of position and velocity. In what follows, the Fourier transforms and the power spectra are given in frequency units. The Fourier transform of velocity is

$$F_v = F_{v'} + F_l^\gamma,$$

where F_l^γ the Fourier transform of the linear trend in velocity, $F_l^\gamma = -i\gamma/\nu$.

The power spectrum of velocity is

$$\begin{cases} P_v = P_{v'} + P_l^{\gamma} + [F_{v'} F_l^{\gamma *} + F_{v'}^{*} F^{\gamma}] \\ \quad = P_{v'} + P_l^{\gamma} + \dfrac{i\gamma}{\nu} [F_{v'} - F_{v'}^{*}], \end{cases} \tag{A1}$$

where asterisks denote complex conjugate.

The Fourier transform of the linearly detrended position time series is

$$F_{\tilde{x}} = F_{x'} + F_l^{c-\kappa} + F_p^{1/2\gamma},$$

where $F_p^{1/2\gamma}$ denotes the Fourier transform of the parabolic trend in position, that is, $F_p^{1/2\gamma} = -\gamma/\nu^2$ and

$$F_l^{c-\kappa} = \frac{i(c-\kappa)}{\nu} = \frac{i\gamma T}{2\nu}.$$

The power spectrum is

$$P_{\tilde{x}} = P_{x'} + P_l^{-\gamma T/2} + P_p^{1/2\gamma}, \tag{A2}$$

and remaining terms in the power spectrum can be checked to cancel out.

We want to assess under which conditions $\nu^2 P_{\tilde{x}} = P_v$. We have

$$\begin{cases} P_{v'} = P_{x'} \nu^2 \\ P_l^{\gamma} = P_p^{1/2\gamma} \nu^2, \end{cases}$$

therefore

$$\begin{cases} \nu^2 P_{\tilde{x}} - P_v = \nu^2 P_l^{-\gamma T/2} - \dfrac{\gamma}{\nu} [F_{v'} - F_{v'}^{*}] \\ \qquad = \gamma \left[\gamma \dfrac{T^2}{4} - \dfrac{i}{\nu} (F_{v'} - F_{v'}^{*}) \right]. \end{cases}$$

Therefore for stationary velocity time series, that is, for no mean acceleration of particles ($\gamma = 0$), one should verify $P_v = \nu^2 P_{\tilde{x}}$ and conversely that $P_v \neq \nu^2 P_{\tilde{x}}$ means that we are dealing with nonstationary velocity because of the presence a net mean acceleration of the flow, which is linked to the existence of a strong mean large-scale circulation.

APPENDIX B

Error Estimate on Velocity Spectra

We assume that the determination of float positions is affected by a white noise error distributed between 0 and 1 km. The corresponding maximal error on velocity time series will therefore be ~ 2 cm s^{-1}. The noise spectrum $B(\nu)$ is

$$B(\nu) = C\nu^2, \tag{B1}$$

and the normalization constant is such that

$$\sum_i^N C\nu_i^2 = (2 \text{ cm s}^{-1})^2,$$

where

$$N = 128 \quad \nu_i = \frac{i}{256 \text{ days}},$$

$$\left(\frac{1}{256 \text{ days}}\right)^2 C \sum_{i=1}^{128} i^2 \sim 4 \text{ cm}^2 \text{ s}^{-2}$$

$$\sum_{i=1}^{128} i^2 = 707264 = M,$$

so that C is given by

$$C \sim 4.0(256)^2/M[(\text{days cm s}^{-1})^2]$$

$$\sim 0.37[(\text{days cm s}^{-1})^2].$$

The error spectrum (B1) corresponds to the dashed line in Figs. 3a and 3b.

REFERENCES

Babiano, A., C. Basdevant, and R. Sadourny, 1985: Structure functions and dispersion laws in two-dimensional turbulence. *J. Atmos. Sci.*, **42,** 942–949.

——, ——, P. Le Roy, and R. Sadourny, 1987: Single-particle dispersion, Lagrangian structure function and Lagrangian energy spectrum in two-dimensional incompressible turbulence. *J. Mar. Res.*, **45,** 107–131.

Brown, M. G., and K. B. Smith, 1990: Are SOFAR floats trajectories chaotic? *J. Phys. Oceanogr.*, **20,** 139–149.

Davis, R. E., 1983: Oceanic property transport, Lagrangian particle statistics and their prediction. *J. Mar. Res.*, **41,** 163–194.

——, 1991: Observing the general circulation with floats. *Deep-Sea Res.*, **38,** S531–S571.

Elhmaidi, D., A. Provenzale, and A. Babiano, 1993: Elementary topology of two-dimensional turbulence from a lagrangian viewpoint and single particle dispersion. *J. Fluid Mech.*, **257,** 533–558.

Griffa, A., K. Owens, L. Piterbarg, and B. Rozovskii, 1995: Estimates of turbulence parameters from Lagrangian data using a stochastic particle model. *J. Mar. Res.*, **53,** 371–401.

Hua, B. L., and D. Haidvogel, 1986: Numerical simulations of the vertical structure of quasi-geostrophic turbulence. *J. Atmos. Sci.*, **43,** 2923–2936.

Isichenko, M. B., 1992: Percolation, statistical topography, and transport in random media. *Rev. Mod. Phys.*, **64**(4), 961–1043.

Middleton, J., 1985: Drifter spectra and diffusivities. *J. Mar. Res.*, **43,** 37–55.

Osborne, A. R., A. D. Kirwan, A. Provenzale, and L. Bergamasco, 1986: A search for chaotic behaviour in large and mesoscale motions in the Pacific Ocean. *Physica D,* **23D,** 75–83.

——, ——, ——, and ——, 1989: Fractal drifter trajectories in the Kuroshio extension. *Tellus,* **41A,** 416–435.

Owens, W. B., 1991: A statistical description of the mean circulation and eddy variability in the western North Atlantic using SOFAR floats. *Progress in Oceanography,* Vol. 28, Pergamon, 257–303.

Panchev, S., 1971: *Random Functions and Turbulence.* Pergamon, 442 pp.

Price, J. F., T. K. McKee, W. B. Owens, and J. R. Valdes, 1987: Site L SOFAR Float Experiment, 1982–1985. Woods Hole Oceanographic Institution Tech. Rep., WHOI-87-52, 289 pp.

Provenzale, A., A. R. Osborne, A. D. Kirwan, and L. Bergamasco, 1991: The study of fluid parcel trajectories in large-scale ocean flows. *Nonlinear Topics in Ocean Physics,* A. R. Osborne, Ed., Elsevier, 367–402.

Richardson, P. L., J. Price, W. B. Owens, W. J. Schmitz, H. T. Rossby, A. M. Bradley, J. R. Valdes, and D. C. Webb, 1981: North Atlantic subtropical gyre: SOFAR floats tracked by moored listening stations. *Science,* **213,** 435–437.

Sanderson, B. G., and D. A. Booth, 1991: The fractal dimension of drifter trajectories and estimates of horizontal eddy-diffusivity. *Tellus,* **43,** 334–349.

Taylor, G. I., 1921: Diffusion by continuous movements. *Proc. London Math. Soc. Ser. 2,* **20,** 196–212.

Wunsch, C., 1982: Low-frequency variability of the sea. *Evolution of Physical Oceanography,* B. Warren and C. Wunsch, Eds., The MIT Press, 623 pp.